

Article

Study of the Structure, Electronic and Optical Properties of BiOI/Rutile-TiO₂ Heterojunction by the First-Principle Calculation

Zhan Qu ¹, Yali Su ², Li Sun ¹, Feng Liang ^{1,*} and Guohe Zhang ^{1,*}

¹ School of Microelectronics, Xi'an Jiaotong University, Xi'an 710049, China; zhanqu@snnu.edu.cn (Z.Q.); sl-lxa@mail.nwpu.edu.cn (L.S.)

² School of Mechanical Engineering, Xi'an Shiyou University, Xi'an 710065, China; sylemon@163.com

* Correspondence: fengliang@xjtu.edu.cn (F.L.); zhangguohe@xjtu.edu.cn (G.Z.)

Received: 18 December 2019; Accepted: 6 January 2020; Published: 10 January 2020



Abstract: Using the first-principle calculation that is based on the density functional theory (DFT), our group gains some insights of the structural, electronic and optical properties of two brand new types of BiOI/TiO₂ heterojunctions: 1I-terminated BiOI {001} surface/TiO₂ (1I-BiOI/TiO₂) and BiO-terminated BiOI {001} surface/TiO₂ (BiO-BiOI/TiO₂). The calculation illustrates that BiOI/TiO₂ heterojunction has excellent mechanical stability, and it shows that there is a great possibility for the BiOI/TiO₂ heterojunction to be used in visible-light range, hence the photocatalytic ability can be enhanced dramatically. Especially, from the calculation, we discovered that there are two specific properties: the band-gap of 1I-BiOI/TiO₂ heterojunction reduces to 0.28 eV, and the BiO-BiOI/TiO₂ semiconductor material changes to n-type. The calculated band offset (BOs) for 1I-BiOI/TiO₂ heterojunction indicates that the interfacial structure contributes a lot to a suitable band alignment which can disperse the photo-generated carriers into the opposite sides of the interface, so this could effectively weaken the electron-hole recombination. Meanwhile, the built-in potential around the interface accelerates the movement of the photo-generated electron-hole pairs. We believe this is the reason that the BiOI/TiO₂ material shows perfect photocatalytic performance. This paper can provide theoretical support for the related research, especially the further research of the BiOI-based material.

Keywords: heterojunction; electronic structure; band offset; photoresponse; first-principles

1. Introduction

In modern environmental engineering, photocatalyst has been widely used for activities such as pollution degradation. Titania (TiO₂) is a typical candidate, and it has received much attention. Besides environmental engineering, it has been used in many fields like photovoltaics. TiO₂ has perfect properties, such as non-toxic, low-cost and great chemical stability [1–3]. But for the energy band properties, TiO₂ is a wide band-gap oxide-semiconductor (3.0 eV for rutile, 3.2 eV for anatase), shows photocatalytic activity under the ultra-violet part of the solar spectrum ($\lambda < 384$ nm). This accounts for only a small portion (5%) of the solar energy. This is the reason that the wide bandgap greatly limits its performance of photocatalytic-degradation [4]. Besides, the rapid recombination of photo-induced electron-hole pairs greatly reduces the quantum efficiency of the system and making its photo-generated quantum-yield to be very low [5–9]. Therefore, it is essential for the researchers to develop effective methods of narrowing the band-gap to the visible-light range and improving the charge-separation efficiency of TiO₂. Therefore, it is highly possible that TiO₂ could be used as an excellent photocatalyst for environmental engineering.

Forming two different semiconductor layers into a heterostructure is an effective method to improve its properties. Under suitable energy band arrangement, the interface could transfer the

carriers from a lower energy band to a higher energy band. Meanwhile, the heterojunction helps the separation of photo-induced electron-hole pairs and prevents the recombination of electron-hole pairs, which could greatly enhance the photocatalytic efficiency of semiconductor heterostructure. In previous researches, scientists found that constructing an interface structure of TiO_2 with a narrow-gap material, such as CdS [10,11], CdSe [12,13], CdTe [10], and Cu_2O [14,15] was considered as a possible method. Under visible-light irradiation, the electron excited from the narrower bandgap semiconductor then transfers to the conduction band of TiO_2 , which can intensify the carrier's transfer and enhances the photocatalytic ability significantly [15–17].

Zhang et al. applied a new approach to compose the bismuth oxyhalide BiOX ($X = \text{Cl}, \text{Br}, \text{I}$) nanospheres [18]. The BiOX with a special layer structure exhibits excellent catalytic properties of degrading pollutants under visible light irradiation. Among those BiOX structures, BiOI is a kind of typical p-type semiconductor with a narrow bandgap of 1.85 eV. It has drawn a lot of attention due to its excellent mechanical and catalytic properties [19–22]. However, its application is affected by the high carrier-recombination probability. This is a severe bottleneck for the use of BiOI . Due to all these reasons, we hypothesize that the combination of BiOI and TiO_2 into a heterojunction might be a wonderful method to overcome the different disadvantages of the two kinds of semiconductors.

In previous experiments, BiOI/TiO_2 heterojunction has been synthesized and demonstrated excellent photocatalytic performance. It is shown that the performance is better than single BiOI or single TiO_2 [4,23]. However, there is limited theoretical research on BiOI/TiO_2 heterojunction. Especially on the aspect of structural stability, electronic structure, and photocatalytic properties. Due to the absence of relevant theoretical modeling research, it is difficult to further the research of the structure and the photo-catalytic ability. Therefore, we make a theoretical study based on the first-principle method to explore the photocatalytic mechanism of BiOI/TiO_2 heterojunctions in this paper.

2. Computation Detail and Models

This research is conducted using Materials Studio software (CASTEP) based on the DFT method. Perdew-Burke-Ernzerhof PBE function of the generalized gradient approximation (GGA) method is used to process the exchange correlation energy [24,25]. A plane-wave cutoff energy (Ecutoff) of 410 eV and ultra-soft pseudo-potential are adopted in the reciprocal K space. A $6 \times 6 \times 1$ Monkhorst-Pack [26] mesh grid is found to be enough to reach convergence for bulk supercell calculations. All the atoms of the heterojunction are fully relaxed to their equilibrium positions with an energy convergence of 5×10^{-6} eV and the atomic displacement is less than 5×10^{-4} Å. The calculated parameters have been tested to be credible to get a convergent result in the work. The pseudo-potentials used for the heterojunction are constructed by the electron configurations as Bi-6s6p, O-2s2p, I-5s5p, and Ti-3d4s for the ground-state of electronic structure calculations [27].

TiO_2 exists in three crystalline polymorphs (anatase, rutile, and brookite). Figure 1a,b shows the structures of BiOI and rutile- TiO_2 (TiO_2) respectively. For TiO_2 , the lattice constants are $a = b = 4.594$ Å, $c = 2.960$ Å, $\alpha = \beta = \gamma = 90^\circ$ [28]. For BiOI , the lattice constants of BiOI are $a = b = 3.984$ Å, $c = 9.128$, $\alpha = \beta = \gamma = 90^\circ$ [29,30]. Notably, the BiOI is constituted of $[\text{Bi}_2\text{O}_2]^{2+}$ and 2I^{2-} layers through weak Van der Waals forces. So, the BiOI unit cell is prone to be dissociated along the {001} direction. In a recent study, Kong et al. [31] studied the properties of three different sections for BiOI {001} surface ({001}-1I, {001}-BiO and {001}-2I) by using first-principles calculations based on DFT within GGA scheme. The calculations results indicate that the {001}-1I facet exhibits the smallest surface energy and the best structural stability. Meanwhile, {001}-BiO facet shows the best photocatalytic performance. Those aspects indicate that 1I- BiOI {001} and BiO- BiOI {001} surfaces are the noteworthy model to compose of a heterojunction with TiO_2 . For this reason, 1I-terminated and BiO-terminated of BiOI {001} surface is attempted to construct heterojunction with {001} crystal plane of rutile- TiO_2 .

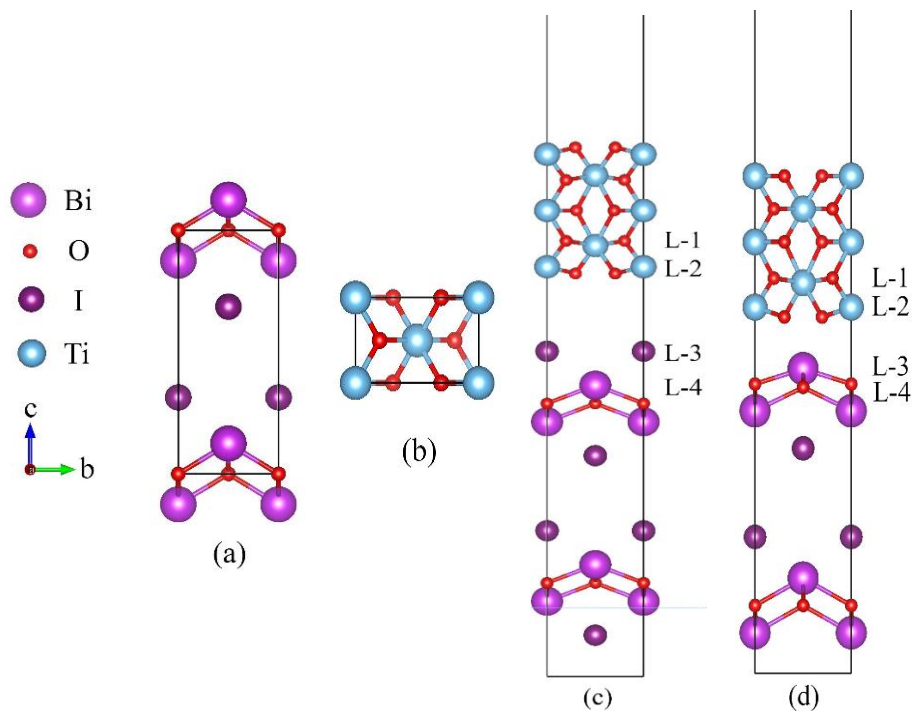


Figure 1. Crystal models: (a) BiOI, (b) rutile-TiO₂, finally relaxed configuration of (c) 1I-BiOI/TiO₂ and (d) BiO-BiOI/TiO₂ heterojunction. Purple, red, brown and blue spheres represent Bi, O, I and Ti atoms respectively. L-1 to L-4 represent atomic layer from layer-1 to layer-4.

It demonstrates that the geometry structures of BiOI {001} surface and TiO₂ {001} surface are equally square. To get a higher matching of BiOI {001} and TiO₂ {001} surfaces, the lattice parameters of the new heterostructure are chosen to be $a = b = 4.289 \text{ \AA}$, which is the average value of the two separate lattice parameters. Thus, the mismatch is only 6.63% for BiOI {001} crystal (along with the X and Y directions). The lattice parameters of the heterojunctions are fixed, whereas the atoms in the materials can relax fully optimization in the calculation. 1I-terminated BiOI {001} surface/TiO₂ (1I-BiOI/TiO₂) and BiO-terminated BiOI {001} surface/TiO₂ (BiO-BiOI/TiO₂) heterojunctions are shown in Figure 1c,d. A 15 Å vacuum region is set to avoid interactions between the top and bottom atoms in the periodic slab images of 1I-BiOI/TiO₂ and BiO-BiOI/TiO₂ heterojunctions. For 1I-BiOI/TiO₂ heterojunction, the whole slab is 38.39 Å contains 25 atoms. The BiOI slab is composed of four layers of Bi atoms, two layers of O atoms and two layers of I atoms. The TiO₂ slab is composed of five atomic layers contain five layers of Ti atoms and five layers of O atoms. For BiO-BiOI/TiO₂ heterojunction, the whole slab is 44.56 Å containing 27 atoms. The BiOI slab is composed of four layers of Bi atoms, two layers of O atoms and four layers of I atoms, and the TiO₂ slab has five atomic layers consisting of five layers of Ti atoms and five layers of O atoms. Finally, the structures, electronic and optical properties of 1I-BiOI/TiO₂ and BiO-BiOI/TiO₂ heterojunctions are systematically investigated according to the density functional theory.

3. Results and Discussion

3.1. The Geometric Structures and Formation Energy of BiOI/TiO₂ Heterojunction

The theoretically optimized model of both 1I-BiOI/TiO₂ and BiO-BiOI/TiO₂ heterojunction is shown in Figure 1c,d.

For the 1I-BiOI/TiO₂ interface (Shown in Figure 1c), the Ti atoms in L-2 are bonded with I atoms in L-3, and the bond length is 4.80 Å. The O atoms in layer-2 are bonded with I atoms in L-3, and the O-I bond length is 4.23 Å. Comparing with unrelaxed heterojunction, the bond length of Ti-I increases by

0.74 Å, and the bond length of O-I increases by 0.75 Å. Meanwhile, the O (L-1)-Ti (L-2) bond length decreases by 0.09 Å, and I (L-3)-Bi (L-4) bond length also decreases by 0.09 Å. The Bi-O bond length and Ti-O bond length away from BiOI/TiO₂ interface increase slightly.

For the BiO-BiOI/TiO₂ heterojunction, as shown in Figure 1d, Ti atoms in L-2 are bonded with O atoms in L-4, and the Ti-O bond length of 3.34 Å. O atoms in L-2 are bonded with Bi atoms in L-4, and the bond length is 2.70 Å. Comparing to the unrelaxed BiO-BiOI/TiO₂ heterojunction, the bond length of Ti-O decreases by 0.23 Å, and the bond length of Bi-O decreases by 0.13 Å. Meanwhile, O (L-1)-Ti (L-2) bond length decreases slightly by 0.09 Å, while Bi (L-3)-O (L-4) bond length also increases by 0.14 Å. Similarly, the Bi-O and Ti-O bond length away from BiOI/TiO₂ interface also increases slightly. When the two materials are combined, the atoms on the BiOI/TiO₂ interface of different materials can generate a force that includes repulsion and attraction, and this will change the bond length of atoms. After the optimization, the bond lengths of Bi-O and Ti-O all increase slightly in the BiOI/TiO₂ heterojunction.

For the BiO-BiOI/TiO₂ heterojunction, as shown in Table 1, the Mulliken's bonding population of O (L-2)-Bi (L-4) bond is 0.08 eV, indicating that Bi-O bonds at the interface have a large part of ionic properties and little covalent properties. Another bond population of Bi-O and Ti-O bonds in the BiOI/TiO₂ interface is zero, which means that ionic property dominates in those bonds.

Table 1. The calculated bond distance (Å) and bond population (e) for the atoms at the interface of the BiOI/TiO₂ heterojunction.

System	Bond	Bond Distance (Å)		Bond Population (e)
		Before Relaxation	After Relaxation	
1I-BiOI/TiO ₂	Ti (L-2)-I (L-3)	4.06	4.80	0
	O (L-2)-I (L-3)	3.48	4.23	0
BiO-BiOI/TiO ₂	Ti (L-2)-O (L-4)	3.57	3.34	0
	O (L-2)-Bi (L-4)	2.82	2.69	0.08

To contrast the structural stability of those two BiOI/TiO₂ heterojunctions, we calculate the formation energy (E_{form}) using the following formula [32]:

$$E_{\text{form}} = \frac{E_{\text{total}} - (E_{\text{BiOI}} + n_{\text{Ti}}\mu_{\text{Ti}} + n_{\text{O}}\mu_{\text{O}})}{A} \quad (1)$$

E_{total} and E_{BiOI} represent the calculated DFT energy for the 1I or BiO terminated BiOI {001} surface model; n_{Ti} and n_{O} represent the numbers of Ti and O atom in TiO₂ slab; μ_{Ti} and μ_{O} are the chemical-potential of the Ti and O atoms; A represents the cross-section area of the interface for the BiOI/TiO₂ heterojunction; μ_{Ti} represents the Ti atomic energy in the bulk Ti; μ_{O} represents half of the total energy of oxygen molecules. The calculated formation energy E_{form} of 1I/TiO₂ and BiO/TiO₂ heterojunctions are $-2.21 \text{ eV}/\text{Å}^2$ and $-2.25 \text{ eV}/\text{Å}^2$, respectively. The E_{form} of the heterojunctions are negative indicating the formations of BiOI/TiO₂ heterojunctions are exothermic and spontaneous, and BiOI and TiO₂ can easily combine. Furthermore, it can be found that BiO-BiOI/TiO₂ is more stable than the 1I-BiOI/TiO₂ heterojunction.

3.2. Electronic Properties

3.2.1. Electronic Structure of BiOI/TiO₂ Heterojunction

The band structures are computed along the special lines connecting the following high-symmetry points: $\Gamma(0,0,0)$, $F(0,0.5,0)$, $Q(0,0.5,0.5)$, $Z(0,0,0.5)$ and $\Gamma(0,0,0)$. Figure 2 demonstrates the band structures for the two heterojunctions. It shows that the conduction band maximum (CBM) for the two types of heterojunctions is at Γ point, while the conduction band minimum (VBM) is at Z point. This indicates the typical characteristic of indirect bandgap material [31]. The band-gap of 1I-BiOI/TiO₂ heterojunction is 0.28 eV. This band-gap is decreased a lot compared to the pure BiOI or the TiO₂.

While for BiO-BiOI/TiO₂ heterojunction, the Fermi level is located at the CBM which means it exhibits the property of n-type semiconductor. A smaller band-gap can produce the redshift phenomenon for 1I-BiOI/TiO₂ heterojunction.

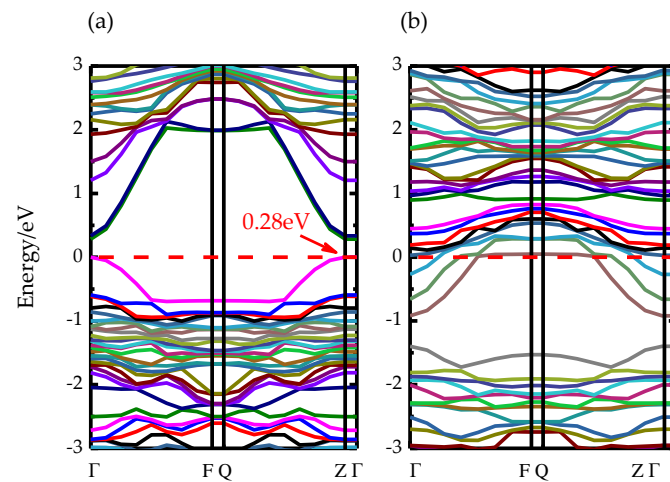


Figure 2. The band structures of relaxed (a) 1I-BiOI/TiO₂, (b) BiO-BiOI/TiO₂ heterojunction. Red dashed line represents the Fermi level.

Due to the lattice mismatch, there exist two kinds of strains. The in-plane biaxial tensile strain ($\varepsilon > 0$) and compressive strain ($\varepsilon < 0$). The strain in the {001} plane of the interface between the BiOI and TiO₂ is induced by the relative difference of lattice constants. The in-plane biaxial tensile strains (IPBTSs) is calculated by the following formula:

$$\varepsilon = \frac{a - a_0}{a_0} = \frac{\Delta a}{a_0} \quad (2)$$

where a and a_0 denote the modified and unmodified lattice constants of the 1I-BiOI/TiO₂ heterojunction respectively. To understand the influence of strain on the electronic properties of 1I-BiOI/TiO₂ heterojunction, we applied a {001} IPBTSs to it. The applied strains vary from -2% to 2% by changing the lattice parameters of 1I-BiOI/TiO₂ heterojunction.

Figure 3 demonstrates the band structures of the 1I-BiOI/TiO₂ heterojunction under different {001} IPBTSs. The band gaps are 0.21 eV, 0.23 eV, 0.30 eV and 0.33 eV for -2% , -1% , 1% and 2% IPBTSs respectively. Notably, the band gaps of those modified materials increase with the increasing strain of the 1I-BiOI/TiO₂ heterojunction; meanwhile, the variation of the band-gap changes are all in the range of 0.12 eV. Therefore, the result of the band gap in our calculation is reliable.

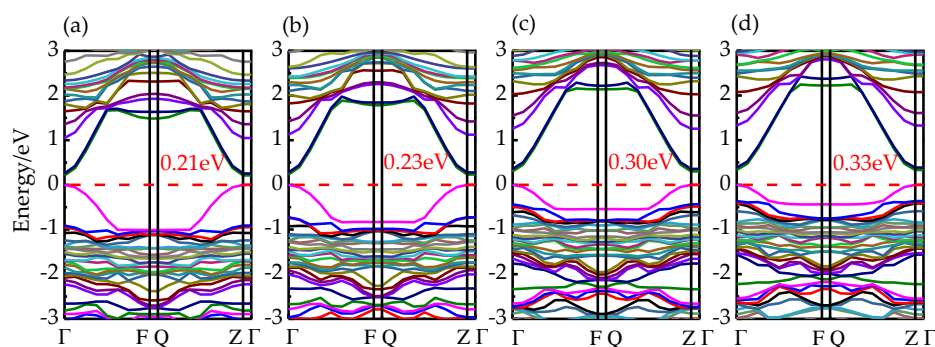


Figure 3. The band structures of 1I-BiOI/TiO₂ heterojunction under (a) -2% , (b) -1% , (c) 1% and (d) 2% {001} IPBTSs. Red dashed line represents the Fermi level.

The total and partial density of states (DOS) for the two heterojunctions depict in Figure 4. It shows the difference between TDOS and PDOS for those heterojunctions. As we can see, in Figure 4, for those two types of heterojunctions, VB is primarily made up of I 5p, O 2p and little Bi 6p states and the VBM is primarily made up of O 2p states, while the CB is chiefly consisted of Bi 6p, Ti 3d, O 2p states. The CBM primarily consists of Bi 6p and Ti 3d states. It reveals that the reason why the photo response for the 1I-BiOI/TiO₂ heterojunction is that the electron transfers from the O 2p in VB to the hybridized Bi 6p and Ti3d states in the CB. Figure 4b presents the DFT-calculated TDOS and PDOS of BiO-BiOI/TiO₂ heterojunction. It can be seen that the CBM downward movement 1.10 eV contrasts to the 1I-BiOI/TiO₂ heterojunction promoting the Fermi level through the CB and makes it an n-type semiconductor.

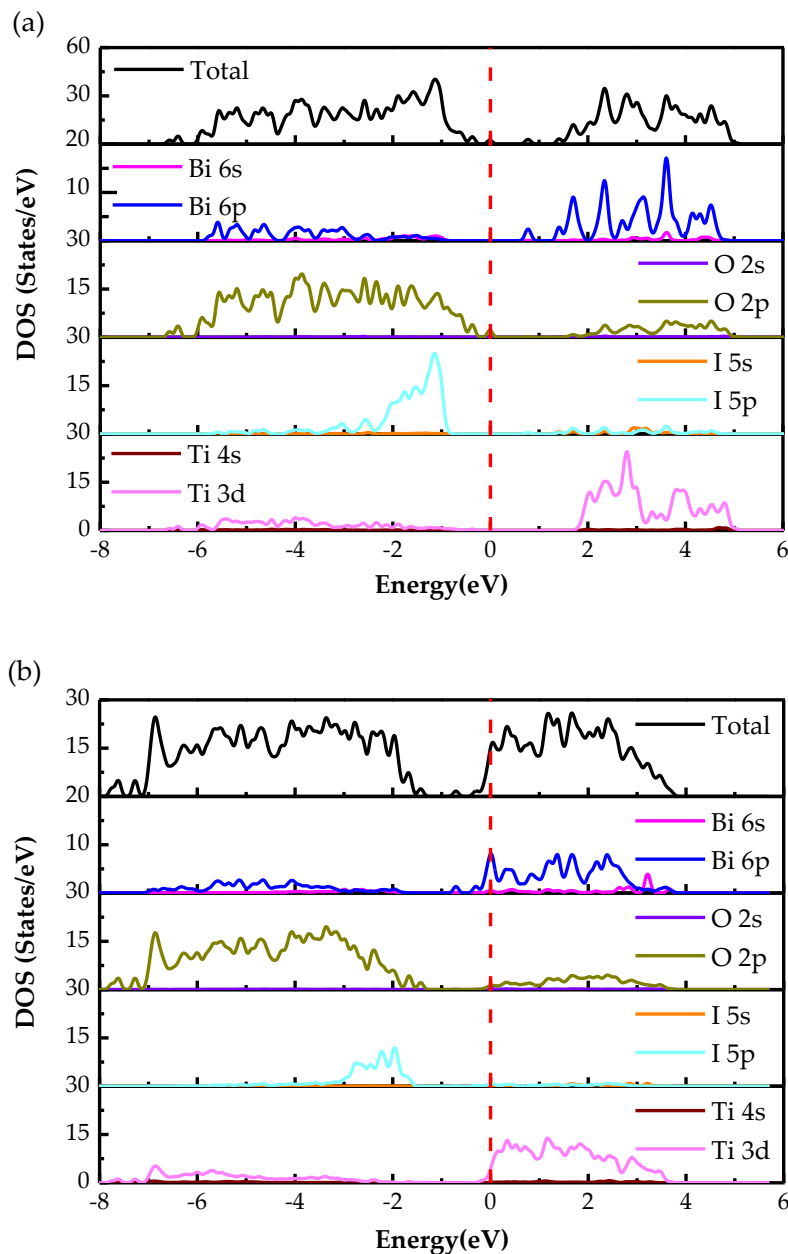


Figure 4. The total and partial density of states of (a) 1I-BiOI/TiO₂, (b) BiO-BiOI/TiO₂ heterojunctions. Red dashed line represents the Fermi level.

3.2.2. Band Offset and Charge Transfer

When two kinds of semiconductors combine into a heterojunction, the band structure of the interface in the heterojunction will form a discontinuous condition. The discontinuous condition finally forms band offset (BOs) (i.e., valence band offset (VBO) and conduction band offset (CBO)). BOs is the most important factor to influence the photo-generated carriers' movement through the interface. Two methods can be applied to obtain the BOs; first is the "local density of states (LDOS)" [33,34] and second is the "potential-line-up methods" [28,35,36]. Here, we use the first approach to obtain the BOs. The second approach is also applied to verify the precision of the BOs of the 1I-BiOI/TiO₂ heterojunction.

The DFT method calculated the density of states, including the TDOS and LDOS regarding bilateral layers far from the interface of the 1I-BiOI/TiO₂ heterojunction that is plotted in Figure 5a. The bulk BiOI and bulk TiO₂, shown in Figure 5a represents the layers far from the interface indicating that the electronic distribution is like that in independent materials. It can be seen from Figure 5a that the valence band and conduction band of bulk BiOI shows a larger shift to the lower energy. In addition, it can be perceived that the band-gap of bulk BiOI is about 1.39 eV, ranging from -0.79 to 0.60 eV, while bulk TiO₂ has a band-gap of 1.91 eV, ranging from 0 to 1.91 eV. The band gap of bulk BiOI and TiO₂ are reduced compared with pure BiOI (1.85 eV) and TiO₂ (3.0 eV). A smaller band-gap of bulk BiOI and TiO₂ will increase the excitation probability of photogenerated electrons, which can stimulate stronger visible light response and enhance the catalytic activity.

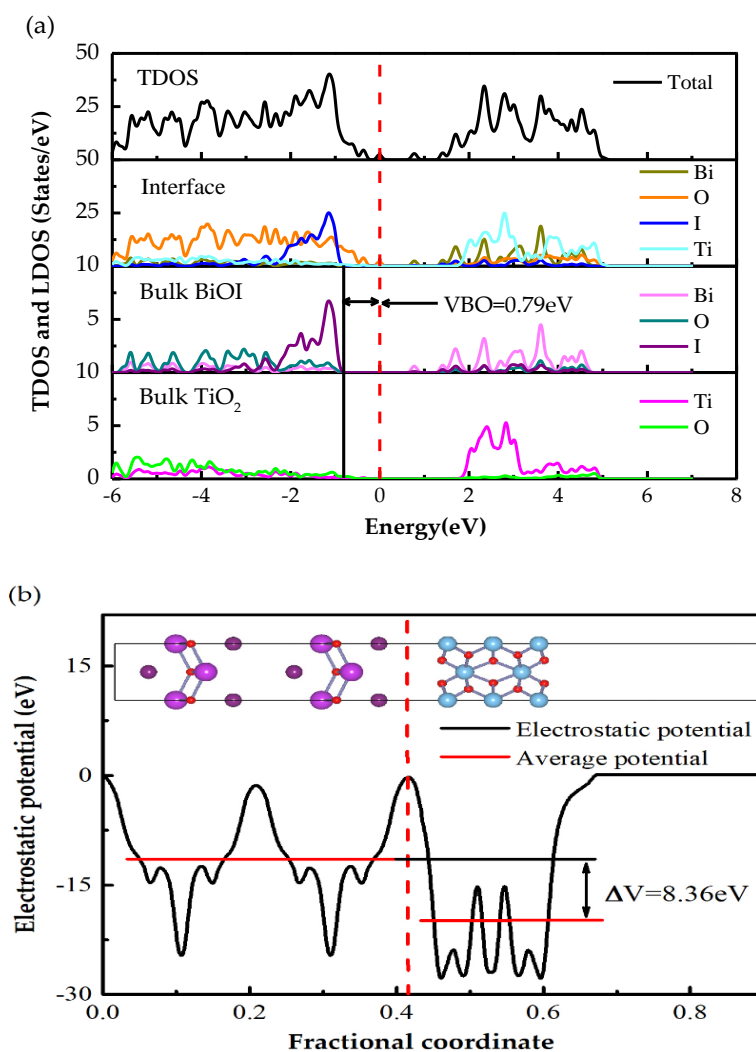


Figure 5. (a) The total and local density of states, (b) electrostatic potential of the 1I-BiOI/TiO₂ heterojunction.

As shown in Figure 5b, the valence band maximum (VBM) of the interface is primarily contributed by TiO₂. The difference VBM between BiOI and TiO₂ is 0.79 eV. Therefore, the VBO between BiOI and TiO₂ is 0.79 eV. Here, the CBO is deduced by utilizing the band gaps of BiOI and TiO₂ from the experiment (3.0 eV for TiO₂ and 1.85 eV for BiOI). The VBO is calculated by the following formula [37–39]:

$$CBO = \Delta E_{gap}^{expt} + VBO \quad (3)$$

ΔE_{gap}^{expt} represents the difference between the experimental optical bands gap of BiOI and TiO₂. The CBO calculated by this formula is 1.94 eV.

The VBO can be deduced through the “potential-line-up method” by the following formula [37,38]:

$$VBO = \Delta E_V + \Delta V \quad (4)$$

ΔE_V is the difference of the VBM got from the pour structures of BiOI and TiO₂ under the same pressure. ΔV is obtained through the calculation of the difference of the average of the electrostatic potential through the 1i-BiOI/TiO₂ heterojunction.

The calculated electrostatic potentials of 1I-BiOI and TiO₂ are plotted in Figure 5b. The solid red lines represent the average potential of BiOI and TiO₂ parts. The average electrostatic potentials of BiOI and TiO₂ are −11.60 eV and −19.96 eV respectively, indicating that ΔV is −8.36 eV. While the VBM of BiOI and TiO₂ are −3.72 eV and 5.67 eV respectively indicating the calculated ΔE_V is 9.39 eV, so the deduced value of VBO is 1.03 eV. The deduced VBO calculated by the potential-line-up method is about 1.03 eV matching well with the value of the LDOS analysis. As shown in Figure 5b, a built-in potential about 28.3 eV is created around the interface of 1I-BiOI/TiO₂ junction. Generally, the calculated VBO and CBO of 1I-BiOI/TiO₂ heterojunction are 0.79 eV and 1.94 eV respectively, which indicates that the BOs between BiOI and TiO₂ will enhance the separation of photogenerated electron-hole pairs and effectively avoid electron-hole recombination. Therefore, electrons could be transferred from the TiO₂ to BiOI section and the holes will be transferred in the opposite direction. In addition, the huge difference of potential through the interface capacity to stimulate separation of electron-hole pairs to the farther ends and finally photocatalytic efficiency can be improved.

A substantial charge transfers through the interfaces of 1I-BiOI/TiO₂ heterojunction. For making a thorough investigation into the electronic distribution and transfer of the 1I-BiOI/TiO₂ heterojunction, the three-dimensional charge density difference (CDD) is used to analyze the properties of 1I-BiOI/TiO₂ heterojunction. CDD can describe the “electronic map” vividly and intuitively. This practical method can be deduced by the following formula:

$$\Delta\rho = \rho_{BiOI/TiO_2} - \rho_{TiO_2} - \rho_{BiOI} \quad (5)$$

$\Delta\rho$, ρ_{TiO_2} and ρ_{BiOI} represent the electronic density of the 1I-BiOI/TiO₂ heterojunction, the free-standing isolated TiO₂ and the 1I-BiOI surface in the same configuration, respectively.

From Figure 6a, we found that there is a dramatic change of the electronic density around the interface owing to the combination of TiO₂ and BiOI. Significant electronic accumulation is observed in the space above I (L-3) atoms in 1I-BiOI part, whereas a little charge depletion is found both on the bottom of Ti (L-2) atoms in the lowest side of the TiO₂ part and the middle of the interface region of the 1I-BiOI/TiO₂ heterojunction. The above analysis indicates that the electron transport violently occurs around the interface owing to the combination of BiOI and TiO₂.

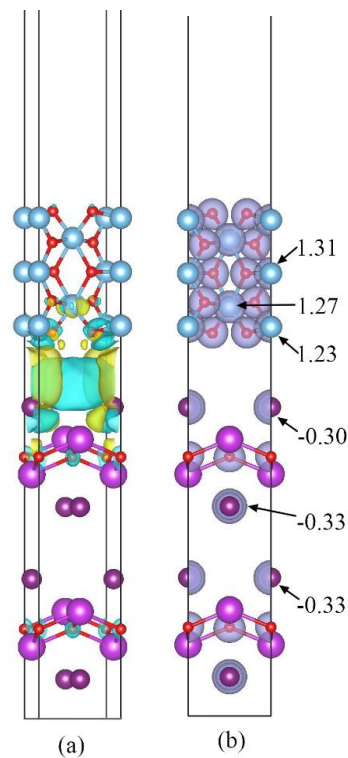


Figure 6. (a) 3D charge density difference for the 1I-BiOI/TiO₂ heterojunction with an isovalue of 0.01 e/Å³. Yellow and cyan isosurfaces represent charge accumulation and depletion in the space respectively. (b) Mulliken population charge distribution maps of 1I-BiOI/TiO₂ heterojunction.

The Mulliken population can present the quantitative calculation of the electronic distribution for the 1I-BiOI/TiO₂ heterojunction. Here, the Mulliken charge of two representative atoms (I and Ti atoms) is demonstrated in Figure 6b. As shown in Figure 6, the I (L-3) atom obtains a Mulliken charge of −0.30, which is greater than I atoms in other layers of 1I-BiOI part, clearly demonstrating that the electron of I atoms (L-3) increases by a very small amount in the 1I-BiOI/TiO₂ heterojunction. The charge variation demonstrates that the I (L-3) atom in the top layer of the BiOI part would lose less electrons than I atoms inside the 1I-BiOI part. While the Mulliken charge of Ti (L-2) is 1.23, which is smaller than Ti atoms in other layers, indicating that the electron redistribution appears around the interface. I (L-3) atoms lose some electrons to Ti (L-4) atoms, indicating that the Mulliken charge analysis is consistent with the CDD analysis. Meanwhile, the built-in potential is created around the interface, and the built-in potential drive electronic transfer from the TiO₂ part to 1I-BiOI part, which is consistent with the band offset analysis in Figure 5a.

3.2.3. Optical Properties and Photocatalytic Mechanism

The dielectric function $\varepsilon(\omega) = \varepsilon_1(\omega) + i\varepsilon_2(\omega)$ provides a close connection between photons and electrons, and it reflects the linear response of materials to electromagnetic radiation [40]. Absorption spectra can be calculated according to the following formula [41]:

$$\alpha(\omega) = \frac{4k\pi}{\lambda_0} = \frac{\omega}{nc} \varepsilon_2(\omega) \quad (6)$$

The calculated optical absorption spectra of pure BiOI, TiO₂ and BiOI/TiO₂ heterojunctions systems as the function of energy and wavelength are displayed in Figure 7. It can obtain that at the low-energy region from 0 to 1 eV, as shown in in Figure 7a, the optical absorption spectra of BiO–BiOI/TiO₂ heterojunction has a small characteristic peak at 0.69 eV. The optical absorption amount of BiOI/TiO₂ heterojunction is much higher than that of pure BiOI and TiO₂ in the low-energy region.

In addition, composing BiOI and TiO₂ into a heterojunction makes the absorption edges redshift, and the BiO–BiOI/TiO₂ heterojunction has a larger amount of redshift than 1I–BiOI/TiO₂ heterojunction. The above analysis makes it clear that the BiOI/TiO₂ heterojunction can dramatically enhance the performance of absorbing visible light, and finally improve the photocatalytic performance.

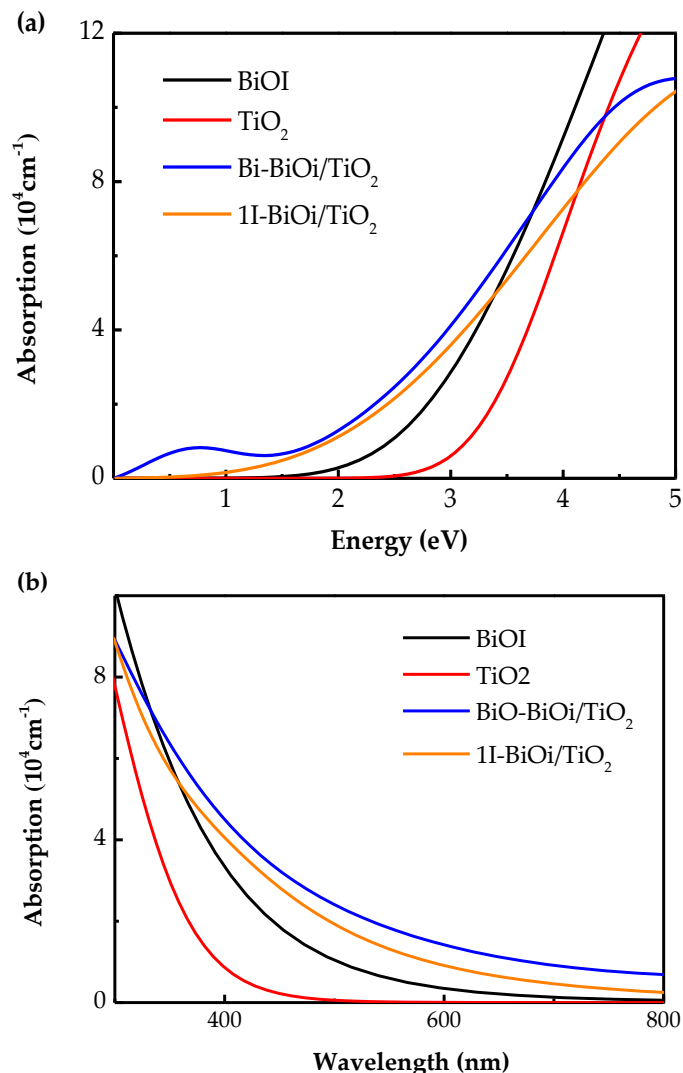


Figure 7. The absorption spectra of pure BiOI, TiO₂, and BiOI/TiO₂ heterojunction as the function of (a) energy and (b) wavelength using the DFT method.

From the above analysis of the electronic structures and optical properties of the 1I–BiOI/TiO₂ heterojunction, a schematic diagram of band structure for pre and post binding 1I–BiOI/TiO₂ heterojunction is shown in Figure 8. We can obtain the conclusions as follows: BiOI with narrow band-gap (1.85 eV) can be tendentiously excited by most of visible light and promote the generation of photoelectrons and holes. However, the generated photo-induced electron-hole pairs of BiOI may recombine immediately due to the narrow band-gap and small sizes, which weakening its photocatalytic properties to a great extent. Because of the large band-gap of TiO₂ (3.0 eV), TiO₂ can only use a few parts of visible-light (energy >2.95 eV, wavelength <420 nm). As shown in the schematic diagram of Figure 8, when BiOI and TiO₂ are contacted with each other constituting a heterojunction, BiOI will play a “photoelectric conversion driver” to absorb visible light. A large built-in potential about 28.3 eV, shown in Figure 5b, and it is created around the interface of the 1I–BiOI/TiO₂ heterojunction. Therefore, electrons could be pumped from the TiO₂ to the BiOI section and the holes will transfer

in the opposite direction. Meanwhile, the built-in potential capacity will promote photogenerated electron-hole pairs separation on the contrary direction.

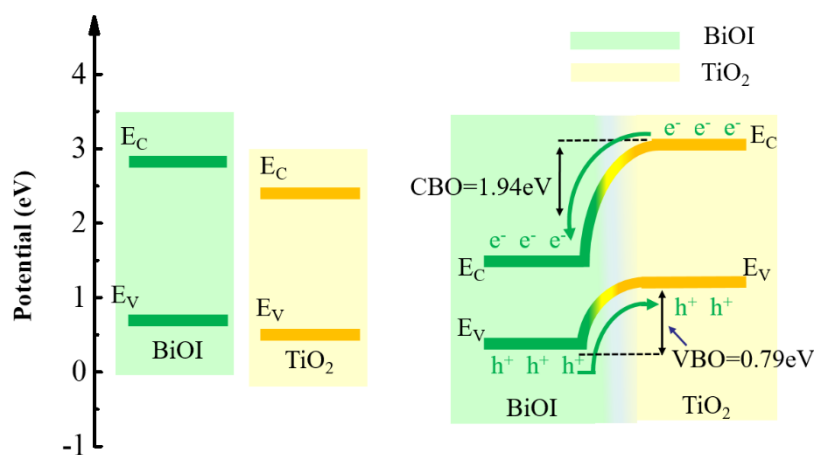


Figure 8. Schematic diagram of the 1I-BiOI/TiO₂ heterojunction and its energy band distribution.

As a result, under the light condition (energy >1.85 eV), photogenic positive holes are stimulated in the VB of p-BiOI part priority. The reformed VB edge of BiOI is more inactive than that of TiO₂ about 0.79 eV. Hence photo-induced holes on the VB of BiOI part would easily transfer to the VB of TiO₂ part while leaving the photo-induced electrons on the CB of BiOI as shown in Figure 8. Electrons will be driven by transferring from CB of TiO₂ to BiOI part driven by built-in potential through the surface at the same time. The formed built-in potential at the interface of 1I-BiOI/TiO₂ heterojunction can significantly accelerate the transfer of photogenerated carriers and prevent its recombination dramatically. The existence of those well-separated photo-electrons and holes would better degrade molecules of organic pollutants. On the whole, the BiOI/TiO₂ heterojunction possesses excellent photocatalytic properties under the degradation of organic pollutants condition under illumination.

4. Conclusions

The characteristics and properties of the 1I-BiOI/TiO₂ heterojunction and the BiO-BiOI/TiO₂ heterojunction are studied via the first-principles calculation based on the DFT theory. The structure of the BiOI/TiO₂ changes slightly, and the interaction on the interface is van der Waals rather than covalent. The band structure of the BiOI/TiO₂ heterojunction is modified a lot. The band-gap of the 1I-BiOI/TiO₂ heterojunction reduces to 0.28 eV and the BiO-BiOI/TiO₂ heterojunction changes into an n-type semiconductor. The calculated VBO of the 1I-BiOI/TiO₂ heterojunction is 0.79 eV, and the CBO of the 1I-BiOI/TiO₂ heterojunction is 1.94 eV respectively. The generated electron-hole pairs will be preferentially produced in the BiOI side under light, and then the holes are easily transferred through the interface from the VBM of the BiOI part to the VBM of the TiO₂ part while leaving the electrons in the CBM of BiOI part. Meanwhile, the built-in potential can effectively speed up the separation of photo-generated electron-hole pairs and effectively avoid electron-hole recombination. Perfectly separated electron-hole pairs across the interface of the BiOI/TiO₂ heterojunction will greatly improve its photocatalytic performance. The conclusions in this paper can provide a theoretical understanding of the BiOI/TiO₂ heterojunction and the further utilization of visible-light response materials, such as BiOI-based semiconductor photocatalysts.

Author Contributions: Conceptualization, Z.Q., Y.S., L.S., F.L. and G.Z.; methodology, Z.Q., Y.S., L.S., F.L. and G.Z.; validation, Z.Q. and G.Z.; formal analysis, Y.S., L.S., F.L. and G.Z.; investigation, Z.Q. and Y.S.; resources, L.S., F.L. and G.Z.; data curation, Y.S. and G.Z.; writing—original draft preparation, Z.Q. and G.Z.; writing—review and editing, Y.S., L.S., F.L. and G.Z.; visualization, Z.Q., Y.S., L.S., F.L. and G.Z.; supervision, Y.S., L.S., F.L. and G.Z. All authors have read and agreed to the published version of the manuscript.

Funding: This research was funded by the National Science Foundation for the Young Scholars of China (Grant No. 61701531).

Conflicts of Interest: The authors declare no conflicts of interest.

References

1. Yu, J.; Fan, J.; Zhao, L. Dye-sensitized solar cells based on hollow anatase TiO₂ spheres prepared by self-transformation method. *Electrochim. Acta* **2010**, *55*, 597–602. [[CrossRef](#)]
2. Jamal, R.; Osman, Y.; Rahman, A.; Ali, A.; Zhang, Y.; Abdiryim, T. Solid-State Synthesis and Photocatalytic Activity of Polyterthiophene Derivatives/TiO₂ Nanocomposites. *Materials* **2014**, *7*, 3786–3801. [[CrossRef](#)] [[PubMed](#)]
3. Hassan, M.E.; Chen, J.; Liu, G.; Zhu, D.; Cai, J. Enhanced Photocatalytic Degradation of Methyl Orange Dye under the Daylight Irradiation over CN-TiO₂ Modified with OMS-2. *Materials* **2014**, *7*, 8024–8036. [[CrossRef](#)] [[PubMed](#)]
4. Dai, G.; Yu, J.; Liu, G. Synthesis and enhanced visible-light photoelectrocatalytic activity of p-n junction BiOI/TiO₂ nanotube arrays. *J. Phys. Chem. C* **2011**, *115*, 7339–7346. [[CrossRef](#)]
5. Hoffmann, M.R.; Martin, S.T.; Choi, W.; Bahnemann, D.W. Environmental applications of semiconductor photocatalysis. *Chem. Rev.* **1995**, *95*, 69–96. [[CrossRef](#)]
6. Yu, J.; Dai, G.; Xiang, Q.; Jaroniec, M. Fabrication and enhanced visible-light photocatalytic activity of carbon self-doped TiO₂ sheets with exposed {001} facets. *J. Mater. Chem.* **2011**, *21*, 1049–1057. [[CrossRef](#)]
7. Xiang, Q.; Yu, J.; Cheng, B.; Ong, H. Microwave-hydrothermal preparation and visible-light photoactivity of plasmonic photocatalyst Ag-TiO₂ nanocomposite hollow spheres. *Chem. Asian J.* **2010**, *5*, 1466–1474. [[CrossRef](#)]
8. Berger, T.; Sterrer, M.; Diwald, O.; Knözinger, E.; Panayotov, D.; Thompson, T.L.; Yates, J.T. Light-induced charge separation in anatase TiO₂ particles. *J. Phys. Chem. B* **2005**, *109*, 6061–6068. [[CrossRef](#)]
9. Kumar, S.; Fedorov, A.G.; Gole, J.L. Photodegradation of ethylene using visible light responsive surfaces prepared from titania nanoparticle slurries. *Appl. Catal. B Environ.* **2005**, *57*, 93–107. [[CrossRef](#)]
10. Sun, W.-T.; Yu, Y.; Pan, H.-Y.; Gao, X.-F.; Chen, Q.; Peng, L.-M. CdS quantum dots sensitized TiO₂ nanotube-array photoelectrodes. *J. Am. Chem. Soc.* **2008**, *130*, 1124–1125. [[CrossRef](#)]
11. Baker, D.R.; Kamat, P.V. Photosensitization of TiO₂ nanostructures with CdS quantum dots: Particulate versus tubular support architectures. *Adv. Funct. Mater.* **2009**, *19*, 805–811. [[CrossRef](#)]
12. Zhang, H.; Quan, X.; Chen, S.; Yu, H.; Ma, N. “Mulberry-like” CdSe nanoclusters anchored on TiO₂ nanotube arrays: A novel architecture with remarkable photoelectrochemical performance. *Chem. Mater.* **2009**, *21*, 3090–3095. [[CrossRef](#)]
13. Kongkanand, A.; Tvrđy, K.; Takechi, K.; Kuno, M.; Kamat, P.V. Quantum dot solar cells. Tuning photoresponse through size and shape control of CdSe-TiO₂ architecture. *J. Am. Chem. Soc.* **2008**, *130*, 4007–4015. [[CrossRef](#)] [[PubMed](#)]
14. Janczarek, M.; Endo, M.; Zhang, D.; Wang, K.; Kowalska, E. Enhanced Photocatalytic and Antimicrobial Performance of Cuprous Oxide/Titania: The Effect of Titania Matrix. *Materials* **2018**, *11*, 2069. [[CrossRef](#)] [[PubMed](#)]
15. Hou, Y.; Li, X.; Zou, X.; Quan, X.; Chen, G. Photoelectrocatalytic activity of a Cu₂O-loaded self-organized highly oriented TiO₂ nanotube array electrode for 4-chlorophenol degradation. *Environ. Sci. Technol.* **2008**, *43*, 858–863. [[CrossRef](#)]
16. Chiou, Y.-K.; Chang, C.-H.; Wang, C.-C.; Lee, K.-Y.; Wu, T.-B.; Kwo, R.; Hong, M. Effect of Al incorporation in the thermal stability of atomic-layer-deposited HfO₂ for gate dielectric applications. *J. Electrochem. Soc.* **2007**, *154*, G99–G102. [[CrossRef](#)]
17. Xu, H.; Ouyang, S.; Liu, L.; Reunchan, P.; Umezawa, N.; Ye, J. Recent advances in TiO₂-based photocatalysis. *J. Mater. Chem. A* **2014**, *2*, 12642–12661. [[CrossRef](#)]
18. Zhang, X.; Ai, Z.; Jia, F.; Zhang, L. Generalized one-pot synthesis, characterization, and photocatalytic activity of hierarchical BiOX (X = Cl, Br, I) nanoplate microspheres. *J. Phys. Chem. C* **2008**, *112*, 747–753. [[CrossRef](#)]
19. Cheng, H.; Huang, B.; Dai, Y. Engineering BiOX (X = Cl, Br, I) nanostructures for highly efficient photocatalytic applications. *Nanoscale* **2014**, *6*, 2009–2026. [[CrossRef](#)]

20. Cao, J.; Xu, B.; Luo, B.; Lin, H.; Chen, S. Novel BiOI/BiOBr heterojunction photocatalysts with enhanced visible light photocatalytic properties. *Catal. Commun.* **2011**, *13*, 63–68. [[CrossRef](#)]
21. Xiao, X.; Zhang, W.-D. Facile synthesis of nanostructured BiOI microspheres with high visible light-induced photocatalytic activity. *J. Mater. Chem.* **2010**, *20*, 5866–5870. [[CrossRef](#)]
22. Cao, J.; Xu, B.; Lin, H.; Luo, B.; Chen, S. Novel heterostructured Bi₂S₃/BiOI photocatalyst: Facile preparation, characterization and visible light photocatalytic performance. *Dalton Trans.* **2012**, *41*, 11482–11490. [[CrossRef](#)] [[PubMed](#)]
23. Zhang, X.; Zhang, L.; Xie, T.; Wang, D. Low-temperature synthesis and high visible-light-induced photocatalytic activity of BiOI/TiO₂ heterostructures. *J. Phys. Chem. C* **2009**, *113*, 7371–7378. [[CrossRef](#)]
24. Segall, M.; Lindan, P.J.; Probert, M.A.; Pickard, C.J.; Hasnip, P.J.; Clark, S.; Payne, M. First-principles simulation: Ideas, illustrations and the CASTEP code. *J. Phys. Condens. Matter* **2002**, *14*, 2717. [[CrossRef](#)]
25. Perdew, J.P.; Burke, K.; Ernzerhof, M. Generalized gradient approximation made simple. *Phys. Rev. Lett.* **1996**, *77*, 3865. [[CrossRef](#)]
26. Monkhorst, H.J.; Pack, J.D. Special points for Brillouin-zone integrations. *Phys. Rev. B* **1976**, *13*, 5188. [[CrossRef](#)]
27. Shanno, D.F.; Phua, K.-H. Matrix conditioning and nonlinear optimization. *Math. Program.* **1978**, *14*, 149–160. [[CrossRef](#)]
28. Colombo, L.; Resta, R.; Baroni, S. Valence-band offsets at strained Si/Ge interfaces. *Phys. Rev. B* **1991**, *44*, 5572. [[CrossRef](#)]
29. Yu, C.; Fan, C.; Jimmy, C.Y.; Zhou, W.; Yang, K. Preparation of bismuth oxyiodides and oxides and their photooxidation characteristic under visible/UV light irradiation. *Mater. Res. Bull.* **2011**, *46*, 140–146. [[CrossRef](#)]
30. Zhao, L.; Zhang, X.; Fan, C.; Liang, Z.; Han, P. First-principles study on the structural, electronic and optical properties of BiOX (X = Cl, Br, I) crystals. *Physica B* **2012**, *407*, 3364–3370. [[CrossRef](#)]
31. Kong, T.; Wei, X.; Zhu, G.; Huang, Y. First-principles studies on facet-dependent photocatalytic properties of BiOI {001} surface. *J. Mater. Sci.* **2017**, *52*, 5686–5695. [[CrossRef](#)]
32. Finnis, M.; Lozovoi, A.; Alavi, A. The oxidation of NiAl: What can we learn from ab initio calculations? *Rev. Mater. Res.* **2005**, *35*, 167–207. [[CrossRef](#)]
33. Bass, J.; Oloumi, M.; Matthai, C.C. A method for determining band offsets in semiconductor superlattices and interfaces. *J. Phys. Condens. Matter* **1989**, *1*, 10625. [[CrossRef](#)]
34. Robertson, J.; Peacock, P. Bonding and structure of some high-k oxide: Si interfaces. *Phys. Status Solidi B* **2004**, *241*, 2236–2245. [[CrossRef](#)]
35. Baldereschi, A.; Baroni, S.; Resta, R. Band offsets in lattice-matched heterojunctions: A model and first-principles calculations for GaAs/AlAs. *Phys. Rev. Lett.* **1988**, *61*, 734. [[CrossRef](#)]
36. Junquera, J.; Cohen, M.H.; Rabe, K.M. Nanoscale smoothing and the analysis of interfacial charge and dipolar densities. *J. Phys. Condens. Matter* **2007**, *19*, 213203. [[CrossRef](#)]
37. Cao, R.; Zhang, Z.; Wang, C.; Li, H.; Xie, X.; Dong, H.; Liu, H.; Wang, W. Interfacial bonding and electronic structure of GaN/GaAs interface: A first-principles study. *J. Phys. D Appl. Phys.* **2015**, *117*, 135302. [[CrossRef](#)]
38. Yang, W.; Wen, Y.; Zeng, D.; Wang, Q.; Chen, R.; Wang, W.; Shan, B. Interfacial charge transfer and enhanced photocatalytic performance for the heterojunction WO₃/BiOCl: First-principles study. *J. Mater. Chem. A* **2014**, *2*, 20770–20775. [[CrossRef](#)]
39. Peressi, M.; Binggeli, N.; Baldereschi, A. Band engineering at interfaces: Theory and numerical experiments. *J. Phys. D Appl. Phys.* **1998**, *31*, 1273. [[CrossRef](#)]
40. Lovell, R. Application of Kramers-Kronig relations to the interpretation of dielectric data. *J. Phys. C. Solid State Phys.* **1974**, *7*, 4378–4384. [[CrossRef](#)]
41. Saha, S.; Sinha, T.P.; Mookerjee, A. Electric Structure, Chemical Bonding, and Optical Properties of Paraelectric BaTiO₃. *Phys. Rev. B* **2000**, *62*, 699–702. [[CrossRef](#)]

